Catalysis Today xxx (xxxx) xxx–xxx

Contents lists available at ScienceDirect

Catalysis Today

journal homepage: www.elsevier.com/locate/cattod

NOx uptake and release on Pd/SSZ-13: Impact Of Feed composition and temperature

Abhay Gupta[a], Sung Bong Kang[b], Michael P. Harold[a,*]

[a] Department of Chemical & Biomolecular Engineering, University of Houston, Houston, Texas 77204, USA
[b] School of Earth Sciences and Environmental Engineering, Gwangju Institute of Science and Technology, 123 Cheomdan-Gwagiro, Buk-gu, Gwangju, 61005, Republic of Korea

ARTICLE INFO

Keywords:
NOx
Pd
SSZ-13
Ethylene
CO
Diesel

ABSTRACT

The Passive NOx Adsorber (PNA) is an emerging technology to abate cold-start NOx emissions from lean combustion vehicles. Binding sites on Pd-exchanged zeolites adsorb NO at low temperature (< 150 °C) and release NO and NO_2 at higher temperature, enabling their downstream reduction. The impacts of other exhaust components such as H_2O, hydrocarbons (HCs) and CO, along with operating conditions including temperature and flowrate must be quantified and understood in order to develop effective PNA materials. We have conducted a systematic set of experiments of the NOx uptake and release features on Pd-exchanged SSZ-13 in the absence and presence of several diesel exhaust components. The NO uptake approaches NO/Pd ~ 1 for a range of conditions, and along with the generation of NO_2 during NO feed and CO_2 (CH_3CHO) during NO + CO (NO + C_2H_4) co-feed, suggests the reduction of well-dispersed Pd cations. The total NO uptake between 50 and 150 °C is nearly constant but occurs in both lower temperature (< ~120 °C) and higher temperature (> 120 °C) regimes, indicating competition of NO uptake with H_2O. The additions of CO and C_2H_4 increase the lower temperature uptake and higher temperature release of NO, both features desirable for application. In contrast, H_2, dodecane, and toluene have a negligible effect on the NO uptake. During NO uptake the co-generation of NO_2, CO_2 and CH_3CHO, respectively with reductants NO, CO, and C_2H_4, provides evidence for the reduction of Pd^{2+} in the form of $[Pd(OH)]^+$ bound to zeolitic anionic sites $[Al\text{-}O\text{-}Si]^-$ and/or PdO_2 clusters. Supporting DRIFTS (diffuse reflectance infrared Fourier transform spectroscopy) measurements identify several potential surface species that are linked to the multiple NO + NO_2 desorption peaks. Two prospective mechanistic schemes are proposed that are consistent with the uptake/release and DRIFTS data.

1. Introduction

The efficiency and durability of diesel engines makes diesel vehicles the clear choice for commercial use. However, diesel combustion operates lean, as do emerging compression ignition methods such as RCCI (reactive charge compression ignition). This means that the conversion of combustion byproduct NO requires lean catalytic reduction methods. During the past ~15 years NOx emission standards have been increasingly tightened to mitigate the detrimental impact on human health. This has led to the development of urea-based selective catalytic reduction (SCR) [1–3]. The development of Cu-exchanged SSZ-13 SCR catalyst has been successful in meeting current NOx emission standards. The SCR has a minimum operating temperature of 180 °C due to limitations associated with urea dosing and conversion to NH_3 [4–7]. Operation below that temperature such as during the vehicle cold start and low load operation will result in untreated NO, which can represent a large fraction of the emissions [8]. As a result, current state-of-the-art NOx control technologies may not be able to meet the emerging regulations such as U.S. EPA (United States Environmental Protection Agency) Tier 3 standards to be implemented by 2025 [9]. New technologies are needed to convert low temperature NO for diesel and other lean burn combustion methods [8,10].

One promising technology is the Passive NOx Adsorber (PNA), introduced in recent years by researchers at Johnson Matthey Inc. [11–13]. The concept follows that of the well-established hydrocarbon trap (HCT). NO and NO_2 emitted during the vehicle cold start are trapped on an adsorbent and then released at a temperature above 200 °C when the SCR becomes active. Prospective PNA materials include noble metals (Pt, Pd) supported on rare earth oxides or zeolites. Pd-exchanged zeolites (BEA, SSZ-13, and ZSM-5) are superior PNA

* Corresponding author.
E-mail address: mpharold@central.uh.edu (M.P. Harold).

https://doi.org/10.1016/j.cattod.2020.01.018
Received 15 October 2019; Received in revised form 19 December 2019; Accepted 10 January 2020
0920-5861/ © 2020 Elsevier B.V. All rights reserved.

Please cite this article as: Abhay Gupta, Sung Bong Kang and Michael P. Harold, Catalysis Today, https://doi.org/10.1016/j.cattod.2020.01.018

ARTICLE IN PRESS

materials [11–13] due in part to their NOx storage capacity and release characteristics [14]. Chen et al. [12] reported the low temperature adsorption of NOx on Pd/zeolite (BEA, ZSM-5, and SSZ-13) [12].

Research on PNA technology has been active in recent years. Reviews by Lee et al. [15] and Gu and Epling [16] provide comprehensive assessments of PNA technology and associated fundamental issues. Mihai et al. [17] characterized Pd/BEA and Pd/SSZ-13 with different silicon to aluminum ratios (SARs), showing that Pd exists as cations mostly in the 2+ valence and lesser in the 4+ state. Mei et al. [18] used density functional theory (DFT) to show that Pd^{2+} sites are reduced to Pd^{+} when exposed to a CO + NO mixture, leading to NO bound to Pd^{+} and generating CO_2. Khivantsev et al. [19] investigated the effects of Pd loading and Silica to Alumina ratio ($Si:Al_2$) on NO adsorption and reported that $Si:Al_2 < 10$ favors dispersion of Pd. Ryou et al. [20] investigated effect of hydrothermal treatment adsorption of NO at low temperature over Pd/SSZ-13 using H_2-TPR (temperature programmed reduction) and XAFS (X-ray absorption fine structure). They reported that HTA (hydrothermal aging) enhances the Pd dispersion and increases NO uptake at lower temperature. A follow-up study by Lee et al. [21] and Ryou et al. [22] showed that H_2O is essential to achieve a high Pd dispersion during high temperature treatment. Moreover, they showed that at temperatures exceeding ~800 °C for more than 15 h, the catalyst deactivates as a result of Pd sintering. They also showed that interaction between the Pd cations and the framework Al was stronger in SSZ-13 than in ZSM-5. Murata et al. [23] conducted NOx trapping on a modified three-way catalyst (TWC) and found a decrease in cold-start NOx and hydrocarbon emissions. Zheng et al. [24] studied the structure, performance, and adsorption chemistry of Pd-exchanged zeolites and reported the existence of multiple Pd species in those materials, including atomically dispersed Pd in cationic sites of zeolite and PdO_2 and PdO particles on external surfaces. Vu at al. [25] performed uptake experiments on Pd/BEA and found out that CO leads to improvement in the amount of stored NOx. Chakarova et al. [26] also studied the effect of adsorption of NO in presence of CO on Pd/ZSM-5 and reported an increased uptake and possible formation of mixed $Pd^{2+}(CO)(NO)$ species. Khivantsev et al. [27] studied how O_2 and CO improve the NOx storage on Pd/SSZ-13. Among other findings, they interpreted DRIFTS measurements to conclude that the formation of a mixed carbonyl-nitrosyl Pd complex contributes to an improvement in the NOx uptake.

To date there have been few systematic studies of the impact of temperature, H_2O, and hydrocarbons. To this end we report the effects of feed parameters, including feed flowrate and temperature, H_2O, and reductant (NO, CO, C_2H_4, toluene – C_7H_8, dodecane – $C_{12}H_{26}$), on NO uptake and release on Pd/SSZ-13. We show that NO uptake is a complex function of the feed conditions, including temperature, reductant type and concentration, through cationic Pd reduction revealed by the generation of oxidation products. DRIFTS measurements assist in the interpretation of the uptake/release data and in the establishment of an underlying mechanism.

2. Experimental

2.1. Catalyst

The PNA monolith piece used for this study, provided by Johnson Matthey Inc., contained 1 wt. % Pd / SSZ-13 (90 %), Al_2O_3 (10 %), 1.5 g/in^3 monolith. The sample had a length of 3.81 cm and diameter of 2.54 cm, had ~300 open channels, and had 1.76 g of washcoat. The Pd loading corresponds to 94.0 μmole Pd/g washcoat for the sample. Table 1 provides more details on the catalyst.

2.2. Bench scale reactor system

A schematic of the bench scale reactor setup is shown in Fig. S1a of the Supplementary Material (SM). Catalyst samples were loaded into a quartz tube reactor which was contained in a temperature-controlled Lindberg/Blue M™ furnace (Thermo-Scientific). The catalyst temperature was measured by a thermocouple positioned at the axial midpoint of a channel located at center of the monolith cross section. A switching valve directed the continuously flowing feed gas to the reactor or bypass line. All the gases (high purity) were provided by either Matheson or Praxair. The flowrates of the various gases were metered by MKS mass flow controllers. The gas lines were heated to over 100 °C to avoid water condensation. [The dew point of water was estimated for the full feed mixture to be ~70 °C; a temperature exceeding 100 °C was used to avoid water condensation.] Species concentrations were analyzed by an MKS FTIR (MultiGas 2030) which enabled the construction of NOx uptake and release transient profiles (Table 2).

Table 1
Passive NOx Adsorber details.

Length of Monolith	1.5″	3.81 cm
Diameter of Monolith	1″	2.54 cm
Volume of Monolith	1.18 inch^3	19.29 cm^3
Loading	1.5 g/inch^3	0.091 g/cm^3
Mass of Washcoat (Volume*loading)	1.766 g	
Mass of Pd in Washcoat	1 % of Mass of Washcoat	0.01*Mass of Washcoat
Molar Weight of Pd	106.42 g	
Moles of Pd	0.00016595 moles	

2.3. Experimental procedure

Before any experiments the fresh catalyst sample was degreened at 600 °C for 4 h in 12 % O_2 and 6 % H_2O. Prior to each individual experiment the catalyst was pretreated in 12 % O_2, 6 % CO_2, 6 % H_2O and balance N_2 at 600 °C for 20 min. Pretreatment was intended to remove any residual NOx or other species and to enable the initial state of the Pd to be in its fully oxidized state which includes Pd^{2+} and $[Pd(OH)]^{+}$ [14,16,28] according to

$$PdO + 2\,H^{+}Z^{-} \rightarrow Z^{-}\,Pd^{2+}Z^{-} + H_2O \quad (1)$$

$$Pd^{+}Z^{-} + H_2O + \tfrac{1}{2}\,O_2 + \leftrightarrow 2\,[Pd(OH)]^{+}Z^{-} \quad (2)$$

where Z^{-} denotes the zeolite anionic aluminum site $(Al\text{-}O\text{-}Si)^{-}$. We note that the presence of Pd^{4+} in the form of PdO_2 cannot be ruled out [24].

In a typical uptake and release experiment the catalyst was brought to the desired uptake temperature in the range of 70–220 °C. The procedure involved exposing the monolith to the feed gas for 30 min at the prescribed temperature followed by a temperature ramp to the maximum operating temperature of 600 °C in 25 min. The uptake part corresponded to exposure of the sample to NO-containing feed gas at fixed temperature. The release part was conducted under a temperature ramp usually with the same feed gas flowing. As we show later, some NO may be trapped during the release phase. The “Total NOx” concentration is defined as the sum of the NO and NO_2 feed concentrations.

Table 2
Feed Composition used in the simulated diesel exhaust feed.

Components	Species	Simple	Complex
Background gases (B.G.)	O_2	12 %	
	H_2O	6 %	
	CO_2	6 %	
NOx	NO	200 ppm	
Reductants	CO	–	500 ppm
	H_2	–	100 ppm
	C_2H_4	–	200 ppm
	C_7H_8	–	42 ppm
	$C_{12}H_{26}$	–	58 ppm

The area under the effluent NOx concentration was subtracted from the rectangular NOx feed to get the amount of NOx adsorbed (Fig. S2). The rectangular feed area was subtracted from area under the curve for the NOx peaks above the 200 ppm line to get the desorbed NOx. The total NOx uptake was the sum of that adsorbed during the fixed temperature period and during the temperature ramp period. The profile obtained during the temperature ramp provides valuable information about the amount and strength of NO (and NO_2) binding. The uptake and desorption values agreed to within ~5 %. Material balances for Carbon, Oxygen, and Hydrogen could not be accomplished due to the high feed concentrations of CO_2 (6 %), O_2 (12 %), and H_2O (6 %).

Several combinations of feeds were performed to understand the effect of each species in the simulated diesel engine feed. Downstream of the reactor a FTIR measured the concentration of effluent gases. Unless otherwise noted, the total flowrate corresponded to a gas hourly space velocity (GHSV, at STP) in the range of 15,000 h^{-1} (4.82 L/min) to 45,000 h^{-1} (14.5 L/min). The feed gas mixture simulating diesel exhaust contained 500 ppm CO, 100 ppm "liquid HC" [toluene (C_7H_8) @ 42 ppm + dodecane ($C_{12}H_{26}$) @ 58 ppm], 200 ppm C_2H_4, 100 ppm H_2, 200 ppm NO, 12 % O_2, 6 % CO_2, 6 % H_2O and balance N_2. The feed mixture is defined as part of after-treatment protocols [29] for catalyst characterization and performance evaluation under the USDRIVE initiative. Although the amounts of the various gas species may be higher or lower during actual vehicle operation, the study is intended to provide a fundamental understanding using a model feed, and to move towards the optimized catalyst for application. A schematic of the protocol is shown in Fig. S1b.

2.4. In-Situ DRIFTS system

Diffuse-reflectance infrared Fourier transform spectroscopy (DRIFTS) measurements were carried out to identify surface species by monitoring the evolution of specific peaks as a function of temperature and gas feed composition. The measurements were carried out using a Nicolet model 6700 FTIR spectrometer (Thermo-Scientific) equipped with a PRAYING MANTIS™ sample collector. The experiments were conducted with SSZ-13 and Pd(1 %)/SSZ-13 powders. The 50 mg SSZ-13 and 1 %Pd/SSZ-13 samples (~200 μm particle size) were pressed into a pellet (3 mm radius and 2 mm height) and is loaded onto the sample holder. The samples were de-greened at 600 °C for 4 h in the presence of 12 % O_2 and balance N_2. The feed gas was introduced at a total flow rate of 100 ml/min, metered by Bronkhorst mass flow controllers. Before each experiment the sample was pretreated at 600 °C in presence of 12 % O_2 and balance N_2 to so that the catalyst was fully oxidized initially. A background spectra was collected at the start of each experiment. The data analysis computes the ratio of the absorption to background giving the IR spectrum with wavenumbers spanning ~4000 to 1000 cm^{-1}. It is noted that the DRIFTS experiment is not done under the same flow conditions and geometry as the monolith catalyst experiments. For this reason its utility is confined to the identification of likely surface species present but not for quantitative model development.

3. Results and discussion

3.1. NOx uptake and desorption for simple feed

The simple feed was first considered which contained NO in a mixture with 6 % H_2O, 6 % CO_2, and 12 % O_2 with balance N_2. Fig. 1 shows a typical NO uptake (adsorption) and release (desorption) experiment respectively, conducted at a fixed temperature of 100 °C and during a 20 °C/min temperature ramp. The first five minutes of the time trace is when the feed is in the bypass line. Upon switching to the reactor feed line there is a ~5 s period during which the feed traverses the reactor and effluent tubing. (Fig. S3 shows example blank tube data.) The NO eventually breaks through, decreases to a minimum, and then gradually approaches the feed value of 200 ppm. At the commencement of the ramp a second dip in the effluent NO concentration occurs, accompanied by the temporal generation of NO_2. Fig. 1 also reports the total NOx (NO + NO_2) along with the effluent H_2O concentration. The data clearly show the evolution of H_2O above its feed value (6 %) during the initial part of the temperature ramp when the second NO uptake occurs. As we discuss later, the generation of NO_2 suggests the reduction of Pd^{2+} in the form of $[Pd(II)(OH)]^+$ to Pd^+, which should generate the same amount of H_2O. Since the amount of H_2O exceeds this value, this suggests the desorption of H_2O from BAS and/or Pd sites, enabling additional NO uptake.

Further into the temperature ramp the NO concentration eventually exceeds the 200 ppm feed value indicating that it is desorbing. A rather broad peak is evident that spans ~1000s (~17 min) over a temperature range of ~340 °C. In order to more clearly pinpoint the location of individual NO (or NO_2) desorption peaks, the feed NO was turned off at the start of the ramp. This experiment produced two isolated peaks with local maxima at ~150 °C and 360 °C, as indicated by the expanded plot in the lower part of Fig. 1. The two NO peaks indicate that there is at least two different sites with distinct binding energies. We return to this point after presenting more NO uptake and release data.

During the latter stage of the temperature ramp the concurrent decrease in NO and increase in NO_2 effluent concentrations was detected. The onset of this trend is at ~450 °C with the NO conversion approaching 6 % by 500 °C. The sum of the NO and NO_2 concentrations is constant at ~200 ppm. The constant NOx concentration suggests the oxidation of a fraction of the NO to NO_2; i.e., NO + ½ O_2 ⟷ NO_2.

The same NO uptake experiment was conducted using a monolith coated with Pd-free SSZ-13 having the same washcoat loading of 1.5 g/in^3. Negligible NO uptake in the presence of water (Fig. S4) was observed. Comparison of the NOx uptake and TPD profiles of the 1 %Pd/SSZ-13 and SSZ-13 indicates a much higher NOx uptake for the former than the latter. The NO uptake on the Pd/SSZ-13 is clearly associated with the Pd in the presence of water.

3.2. Uptake temperature effect for simple feed

The impacts of several variables were examined for the simple feed starting with the uptake temperature. Fig. 2 shows the uptake and release profiles for NO and NO_2 at multiple uptake temperatures between 70 and 220 °C. The NO data in Fig. 2a and corresponding NO_2 data in Fig. 2b clearly show the existence of four regimes in the 100 °C uptake experiment. The first two regimes of NO uptake (and NO_2 generation) occur at ~300 s and 2300s; the third regime starts at ~2500s and lasts for ~1000s and involves the release primarily of NO; the fourth regime occurs during the last few hundred seconds of the ramp and involves concurrent NO consumption and NO_2 production. Each of the regimes is now considered in more detail.

In the first regime the NO uptake and NO_2 generation increase with uptake temperature, while in the second regime the opposite trend is encountered; i.e., the NO uptake and NO_2 generation decrease with uptake temperature. Fig. 3a reports the integrated NO uptake (in μmol NO/g washcoat) during the first and second regimes. Fig. 3b shows the corresponding NO_2 generation (in μmol NO_2/g washcoat) over the same temperature range. The increases in NO uptake and NO_2 generated are monotonic up to ~180 °C, while for temperatures > 180 °C, the NO uptake and NO_2 generated both decrease monotonically. The sum of the NO uptake in the first and second regimes is also plotted in Fig. 3a. That sum shows a shallow relative minimum at ~90 °C and shallow relative maximum at ~180 °C. As a point of reference, the 1 % Pd/SSZ-13 sample has a loading of 94 μmol Pd/g washcoat; this is indicated as the horizontal dashed line in the Fig. 3a. The total NO_2 generated in the first two regimes is plotted in Fig. 3b, and shows the same two extrema. It is evident that the total NO is confined to a range of 100–115 μmol NO/g washcoat. This range is ~5 – 20 % higher than the loading of Pd in the sample (94 μmol Pd/g washcoat). A Pd/NO ratio of unity implies

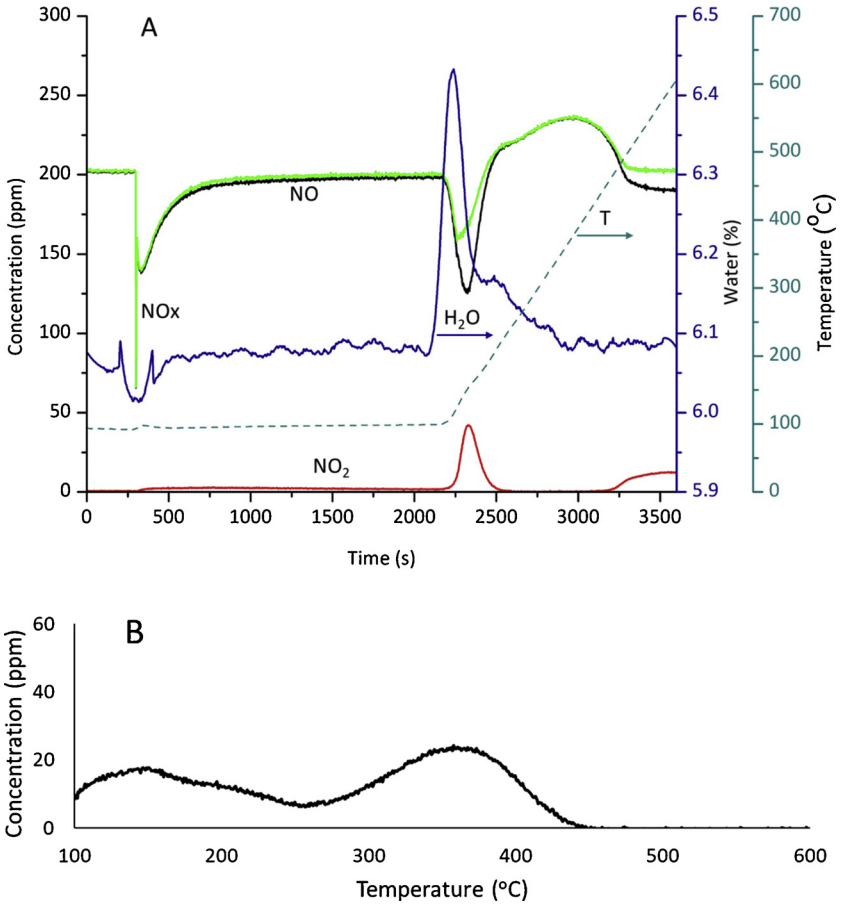

Fig. 1. (a) NOx uptake and release profile at 100 °C. (b) NO desorption profile as function of temperature.
Feed: 200 ppm NO, 6 % H_2O, 6 % CO_2, 12 % O_2, balance N_2; GHSV = 30,000 h^{-1}

that one NO is adsorbed on each isolated Pd cation. A ratio exceeding unity is explained by one or more factors. First, more than one NO may adsorb on a Pd cation; DFT calculations to be reported elsewhere show that more than one NO may bind to a Pd cation, although the desorption temperature of the additional NO's is still to be estimated and measured [30,31]. Second, additional NO uptake may occur on Pd cations or BAS sites from which H_2O has desorbed during the temperature ramp. Third, some NOx uptake may occur in the form of nitrates. We return to these points later.

The limiting NO uptake features of the simple feed containing NO and H_2O helps to explain the trends in the NO uptake data (Fig. 3). For uptake temperatures below ~50 °C (data not shown here) the first NO uptake is negligible. Subsequent exposure of the catalyst to a temperature ramp results in an increase in NO uptake to as high as 110 μmol NO/g washcoat. These limiting features suggest competition between NO and H_2O for adsorption on the Pd cations. At temperatures below 50 °C the H_2O blocks NO uptake whereas at higher temperature the desorption of H_2O frees up sites for NO uptake. We return to this

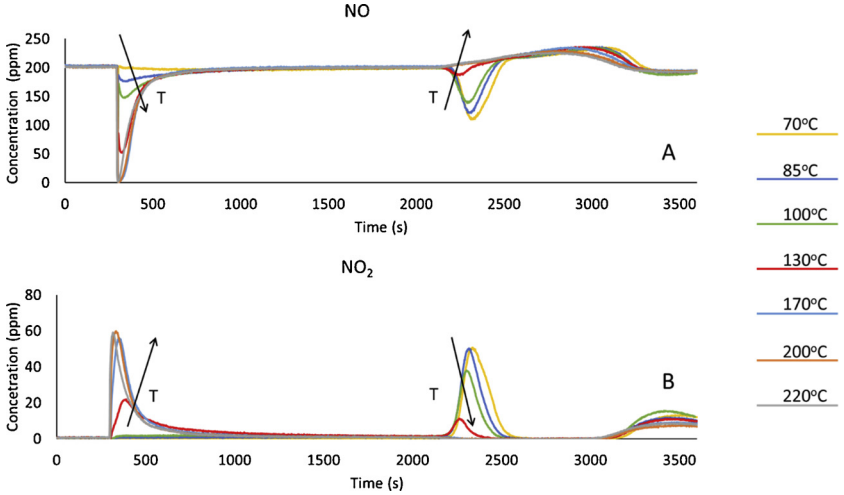

Fig. 2. (a) NO uptake and release profile at several uptake temperatures. (b) NO_2 generation profile at several uptake temperatures.
Feed: 200 ppm NO, 6 % H_2O, 6 % CO_2, 12 % O_2, balance N_2; GHSV = 30,000 h^{-1}

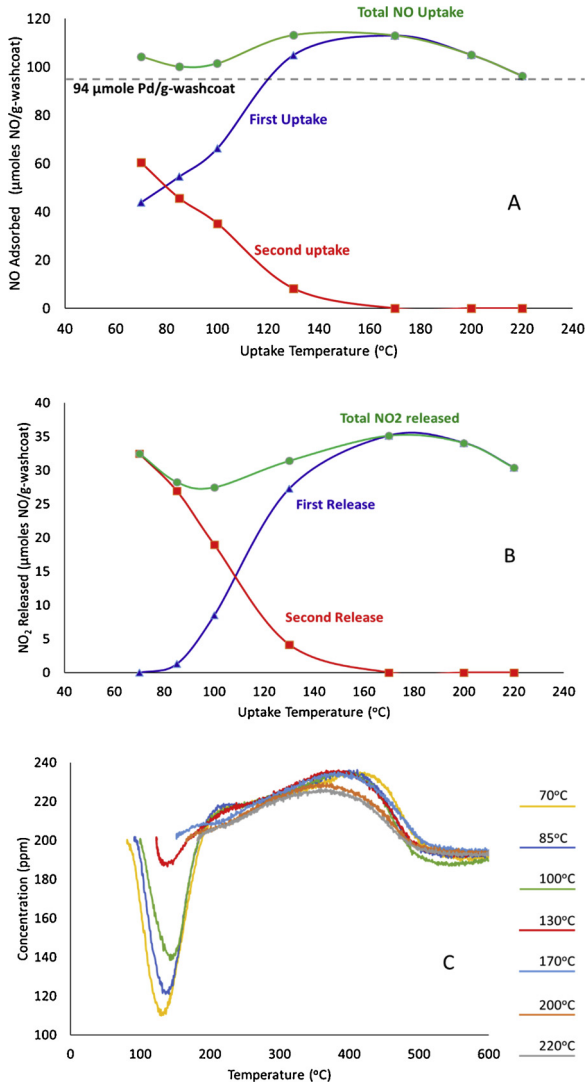

Fig. 3. (a) NO uptake during two regimes as a function of uptake temperature. (b) NO_2 generation during two regimes as a function of uptake temperature. (c) Desorption of NO as function of monolith temperature for several uptake temperatures.
Feed: 200 ppm NO, 6 % H_2O, 6 % CO_2, 12 % O_2, balance N_2; GHSV $=30{,}000\ h^{-1}$

point later.

Fig. 3c shows the effluent NO concentration as a function of temperature for all of the NO uptake experiments. These data shows a NO desorption profile that is nearly independent of the NO uptake temperature. This underscores the fact that the total NO uptake during the first two regimes is essentially constant. Further, not only the amount but also the nature of the binding is essentially independent of the uptake based on the near-overlap of the desorption curves.

The integral NO trapping efficiency $\eta_T(\tau)$ at temperature T and for duration τ, where $\eta_T(\tau)$ is defined as [32]:

$$\eta_T(\tau) = 100\left(1 - \frac{1}{\tau F^o_{NO_x}} \int_0^\tau F_{NO_x}(t)dt\right) \quad (3)$$

This performance metric gauges the ability of the PNA to retain fed NO during the first uptake regime. Fig. S5 reports $\eta_T(\tau)$ versus time for several uptake temperatures (T = 70–170 °C). From an application standpoint, $\eta_T(\tau)$ should be 100 % for the first 2 − 3 min. These data show that for the simple feed this is clearly not the case; i.e. even during the initial part of the uptake there is clearly breakthrough of NO. Thus, in the absence of feed components other than NO, H_2O, and CO_2, the Pd/SSZ-13 is not effective in trapping the NO.

3.3. In-situ DRIFTS with simple feed

DRIFTS measurements provide important information about the identity of surface species. Fig. 4 shows DRIFTS results for NO adsorption at 100 °C during NO exposure to SSZ-13 and Pd(1 %)/SSZ-13 for a dry feed. Table 3 lists the important IR peaks of interest provided in previous studies for NO interacting with SSZ-13 and Pd/SSZ-13 [33].

The SSZ-13 data show a prominent peak at 2170 cm^{-1}, which is attributed to NO^+ adsorbed on the cationic sites of the zeolite (H^+) [33–35]. Chen et al. [36] reported that this peak vanishes in the presence of sufficient H_2O in the feed, and is probably a result of the strong binding of H_2O to BAS of the zeolite. The same 2170 cm^{-1} peak is observed for 1 % Pd-SSZ-13 for the dry feed, indicating that BAS uptake NO and NO_2 when H_2O is not present. A less intense peak at 1643 cm^{-1} is attributed to surface nitrate species (NO_3^-) [14,37] on both protonated and Pd cation bound zeolitic anionic sites. The negative peak at 3610 cm^{-1} is attributed to the consumption of acidic hydroxyls during the NO uptake process [14,38]. The 2170 cm^{-1} and 1643 cm^{-1} peaks suggest that NO is oxidized by O_2 to NO_2 and that further oxidation to nitrates (NO_3^-) occurs. Notwithstanding that these measurements were made for a dry feed, that the 1643 cm^{-1} peak persists in the presence of H_2O indicates that nitrates exist under application relevant conditions. An example spectra is shown in Fig.S6 of the Supplemental Material.

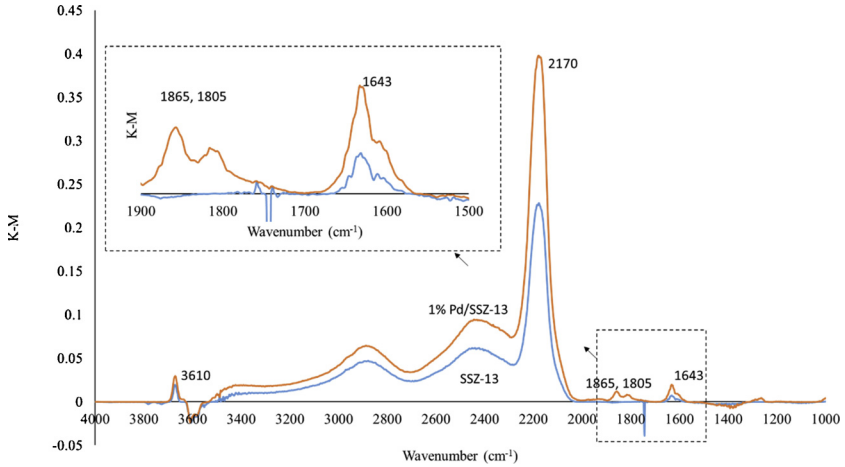

Fig. 4. DRIFTS spectra obtained during NO + O_2 exposure to SSZ-13 and 1 % Pd/SSZ-13. Feed: 1400 ppm NO, 12 % O_2, balance N_2; flow rate $=100$ ml/min. Conditions: 100 °C; Duration 1 h; 50 mg Pd/SSZ-13 powder

Table 3
IR peak assignments for NO + O_2 on 1 %Pd/SSZ-13.

IR Peak (cm^{-1})	Assignment	NO	NO + CO	NO + C_2H_4
1187.1	CH2 rocking and torsion and COH bending vibration may give rise to its intensity.	x	x	✓
1225.6	COH bending of 2-nitrosoethanol	x	x	✓
1482	(ν12, δCH_2 in-plane) vibrations based on C_2H_4 interactions with zeolites	x	x	✓
1587	NOy – C_2H_4 complex being formed. Or N = O stretch of 2-Nitrosoethanol	x	x	✓
1643	Nitrate species on H-SSZ-13	✓	✓	✓
1680	C_2H_4 showing H-C-H vibrations with adsorption on BAS	x	x	✓
1795	NO on Pd^+ after reduction through CO, everything converts to Pd^+	x	✓	x
1805	NO-Pd complex reversibly coordinated species	✓	x	x
1816	NO on Pd^+ after reduction through C_2H_4, everything converts to Pd^+	x	x	✓
1865	NO adsorbed on Pd^{2+}	✓	x	x
2150	CO species in cationic position of zeolites (H^+) (replacing NO)	x	✓	x
2170	(NO^+) species in cationic position of zeolites (H^+) (this peak disappears in presence of Water)	✓	✓	✓
3610	Acid hydroxyls of the zeolite structure being consumed	✓	✓	✓

The two broad peaks spanning ~2300 to ~3300 cm^{-1} are a result of atmospheric water that could not be eliminated from the system [33].

Notably, two smaller peaks at 1865 cm^{-1} and 1805 cm^{-1} were detected for the Pd/SSZ-13 sample but not for the SSZ-13 sample with the dry feed., These peaks persist in the presence of H_2O, indicating their importance for NO uptake (Fig. S6). The 1865 cm^{-1} is attributed to NO adsorbed on Pd^{2+} while the 1805 cm^{-1} peak is attributed to a NO-Pd^+ complex [14,27]. Debate is ongoing regarding assignment of the 1805 cm^{-1} peak. Nevertheless, the collective observations together with DFT calculations are consistent with Pd^{2+} reduction to Pd^+ leading to uptake of strongly-held NO. We expand on this point later.

3.4. Effect of water with simple feed

Water is a ubiquitous exhaust component and its sorption plays an important role during NO uptake at lower temperatures. Specifically, H_2O competes with NO, NO_2 [39] and other exhaust components for adsorption sites and the extent of the blocking is a function of temperature. This is inferred from data shown earlier but can be more explicitly shown by removing water from the feed and assessing the impact. Fig. S4 shows that in the presence of H_2O, SSZ-13 adsorb only a negligible amount of NOx, which is likely the result of site blockage by adsorbed H_2O. When H_2O is removed from the feed at least three times as much NO adsorbs compared to the wet feed NO uptake. This suggests that adsorption occurs on Brønsted acid sites consistent with the literature [18,27]. For Pd(1 %)/SSZ-13, Fig. S7 compares the NO uptake results for two feeds, one with H_2O (6 %) and one without H_2O. When Pd is present, the NO uptake is lower with H_2O in the feed but it is not zero. The uptake comparison shows that the addition of H_2O greatly reduces the amount of NOx adsorbed.

3.5. NO uptake and release schemes for simple feed

The uptake and release data and DRIFTS measurements obtained for the simple feed form the basis for a prospective NO uptake mechanism. In a parallel study of the related NO uptake on Pd/ZSM-5, Ambast et al. [31] propose two mechanistic schemes, discussed in more detail later. Both schemes consider that reduced Pd cations sites are primarily responsible for the NO uptake and conversion. The difference is the identity and valence of the key Pd cations. Scheme I considers that [Pd(OH)]$^+$ is reduced to Pd^+ with NO uptake on Pd^+; Scheme II considers that PdO_2 is reduced to PdO with NO uptake as $Pd(NO_3)_2$ [34]. The Pd reduction step is critical for both schemes. Note that the schemes presented here do not consider NO/NO_2 uptake on Brønsted acid sites since H_2O is a strong inhibitor.

Scheme I, provided in Table 4, involves three cationic Pd species: $Z^-Pd^{2+}Z^-$, $Z^-[PdOH]^+$, and Z^-Pd^+, where Z^- represents the zeolitic anionic site $[Al\text{-}O\text{-}Si]^-$. The existence of three binding sites for NO follows from the uptake and TPD data as well as calculations by density functional theory (DFT). Details are provided by Ambast et al. [31] in a related experimental and modeling study of NO uptake, conversion and release on Pd/ZSM-5; details of the DFT calculations will be reported elsewhere by Menon et al. [30]. The first group of reaction steps, R1 - R7, involve NO and NO_2 binding on H_2O-occupied sites. A key element of this scheme is the reduction of Pd^{2+} given by reaction R8. Evidence for the existence of Pd^+ is the aforementioned 1805 cm^{-1} peak detected by DRIFTS. Additional data provides circumstantial evidence for the proposed mechanism. These are discussed below. At higher temperature, desorption of H_2O, via the reverse of steps R1 – R3, frees up sites for additional NO binding, i.e. steps R9 – R14. Finally, R15 represents re-oxidation of Pd^+ to Pd^{2+}.

Table 4
Mechanistic Schemes I and II.

SCHEME I	
Reaction No	Reaction
R1	$H_2O + Z^-Pd^{2+}Z^- \leftrightarrow Z^-Pd^{2+}Z^- - H_2O$
R2	$H_2O + Z^-[Pd(II)OH]^+ \leftrightarrow Z^-[Pd(II)OH]^+ - H_2O$
R3	$H_2O + Z^-Pd^+ \leftrightarrow Z^-Pd^+ - H_2O$
R4	$NO + Z^-Pd^{2+}Z^- - H_2O \leftrightarrow Z^-Pd^{2+}Z^- - (H_2O)(NO)$
R5	$NO + Z^-[Pd(II)OH]^+ - H_2O \leftrightarrow [Pd(II)OH]^+ - (H_2O)(NO)$
R6	$NO + Z^-Pd^+ - H_2O \leftrightarrow Z^-Pd^+ - (H_2O)(NO)$
R7	$NO_2 + Z^-Pd^{2+}Z^- - H_2O \leftrightarrow Z^-Pd^{2+}Z^- - (H_2O)(NO_2)$
R8	$NO + 2Z^-[Pd(II)OH]^+ \leftrightarrow 2Z^-Pd^+ + NO_2 + H_2O$
R9	$NO + Z^-Pd^{2+}Z^- \leftrightarrow Z^-Pd^{2+}Z^- - NO$
R10	$NO + Z^-Pd^{2+}Z^- - NO \leftrightarrow Z^-Pd^{2+}Z^- - (NO)_2$
R11	$NO + Z^-Pd^{2+}Z^- - (NO)_2 \leftrightarrow Z^-Pd^{2+}Z^- - (NO)_3$
R12	$NO_2 + Z^-Pd^{2+}Z^- \leftrightarrow Z^-Pd^{2+}Z^- - NO_2$
R13	$NO + Z^-[Pd(II)OH]^+ \leftrightarrow Z^-[Pd(II)OH]^+ - NO$
R14	$NO + Z^-Pd^+ \leftrightarrow Z^-Pd^+ - NO$
R15	$2Z^-Pd^+ + Z^-H^+ - H_2O + 0.5O_2 \leftrightarrow 2Z^-[Pd(II)OH]^+ + Z^-H^+$
SCHEME II	
R16	$NO + Z^-Pd^{2+}Z^- \leftrightarrow Z^-Pd^{2+}Z^- - NO$
R17	$NO + Z^-Pd^{2+}Z^- - NO \leftrightarrow Z^-Pd^{2+}Z^- - (NO)_2$
R18	$NO + Z^-Pd^{2+}Z^- - (NO)_2 \leftrightarrow Z^-Pd^{2+}Z^- - (NO)_3$
R19	$NO_2 + Z^-Pd^{2+}Z^- \leftrightarrow Z^-Pd^{2+}Z^- - NO_2$
R20	$NO + PdO_2 \leftrightarrow PdO + NO_2$
R21	$2\,NO + 1.5O_2 + PdO \leftrightarrow Pd(NO_3)2$
R22	$2\,PdO + O_2 \leftrightarrow 2PdO_2$
R23	$H_2O + Z^-Pd^{2+}Z^- \leftrightarrow Z^-Pd^{2+}Z^- - H_2O$
R24	$NO + Z^-Pd^{2+}Z^- - H_2O \leftrightarrow Z^-Pd^{2+}Z^- - (H_2O)(NO)$
R25	$NO_2 + Z^-Pd^{2+}Z^- - H_2O \leftrightarrow Z^-Pd^{2+}Z^- - (H_2O)(NO_2)$
R26	$H_2O + PdO_2 \leftrightarrow PdO_2 - H_2O$
R27	$H_2O + PdO \leftrightarrow Pd(OH)2$

Scheme I is able to predict the following main features of the NO uptake, conversion, and release data:

- *NO/Pd ratio approaching and exceeding 1*. With H_2O in the feed, the measured NO/Pd ~ 1 suggests that all of the Pd is in the form of

isolated cations. NO/Pd exceeding 1 suggests that more than one NO may adsorb on Pd-exchanged sites, supported by DFT calculations [18,24]. As mentioned earlier, experimental evidence of more than one NO adsorbing on Pd exchanged sites is lacking, there may be other contributing factor. These include incremental NO uptake on Pd as H_2O desorbs during the temperature ramp, or NOx uptake in the form of nitrates. Only after prolonged exposure of the Pd/SSZ-13 sample to CO-containing gas were NO/Pd values less than unity observed. That observation suggests a potential deactivation process which has been observed elsewhere [10] but is beyond the scope of the current study.

- *Multiple NO desorption peaks.* NO desorption during the temperature ramp following uptake at lower temperature shows the existence of two or more binding sites (Fig. 1b). Based on DFT calculations [30] the lower temperature NO peak (~150 °C) is NO bound to $Z^{-}Pd^{2+}Z^{-}$ and $Z^{-}[Pd^{2+}OH]^{+}$ with estimated binding energies of 125 and 160 kJ/mole, respectively [33–35]. The higher temperature NO peak (~350 °C) is NO bound to $Z^{-}Pd^{+}$, with an estimated binding energy of 230 kJ/mole.
- *Water inhibition.* Adsorption of H_2O strongly inhibits NO uptake on Brønsted acid sites while it reduces the extent of NO binding on Pd-associated sites. During the temperature ramp the additional NO uptake that occurs is explained by desorption of H_2O [14,36,40], which frees-up Pd cationic binding sites. The NO uptake data show that the sum of NO uptake during the fixed temperature period and during the temperature ramp is nearly constant and equal to the Pd loading. The simplest explanation for this feature is competition between NO and H_2O. While co-adsorption of NO and H_2O is predicted to occur from DFT analysis, the binding of NO on sites devoid of H_2O is higher [18,24]. As a result, during the temperature ramp H_2O desorption occurs followed by NO uptake on those sites.
- *Generation of $NO_2$with NO uptake.* During NO uptake NO_2 generation is detected for the simple feed. This suggests a chemical reduction of Pd cations by NO which serves as a reductant in the simple feed. Step R8 represents an overall reaction involving the reduction of two $[PdOH]^{+}$ [14] yielding one surface nitrosyl ($Pd^{+}NO$) and NO_2. With adsorption of an additional NO the following overall reaction applies:

$$3\ NO + 2Z^{-}[Pd^{2+}(II)OH]^{+} \leftrightarrow 2\,Z^{-}Pd^{+}\ NO + NO_2 + H_2O \qquad (R28)$$

(Note that R28 = R8 + 2R14.) Thus, every NO_2 generated involves the reduction of two $[Pd(OH)]^{+}$ species. The stoichiometry enables an estimation of the fraction of the total adsorbed NO that is in the form of $Pd^{+}NO$. Fig. 5 shows the measured NO_2 that is generated along with the total NO uptake at several temperatures. For the Pd loading of 94 μmole/g washcoat, a maximum NO_2 generation rate of 47 μmole NO_2/g washcoat is possible assuming all of the NO adsorbs on Pd^{+} sites. The actual NO_2 generation rate of 30 μmole NO_2/g washcoat means that 64 % of the adsorption sites are the form of $Z^{-}[Pd(OH)]^{+}$ and $Z\text{-}Pd^{+}$ while the remaining 36 % in the form of $Z^{-}Pd^{2+}Z^{-}$.

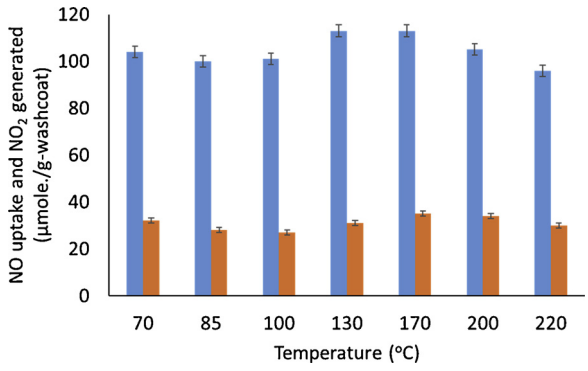

Fig. 5. Total NO uptake (blue; left bar) and NO_2 generated (orange; right bar) in μmole/g washcoat. (For interpretation of the references to colour in this figure legend, the reader is referred to the web version of this article). (For interpretation of the references to colour in this figure legend, the reader is referred to the web version of this article).

While Scheme I is able to explain the NOx uptake features on Pd/SSZ-13 and is supported by DRIFTS measurements, definitive proof remains elusive. For example, Scheme I does not consider Pd in the form of PdO or PdO_2 clusters or particles, which others have contended exist [24]. Moreover, as mentioned earlier, the IR assignment of Pd^{+} at 1805 cm^{-1} remains under debate [16]. To this end, Scheme II also proposed by Ambast et al. [31] and provided in Table 4, considers that NO uptake occurs only on $Z\text{-}Pd^{2+}Z\text{-}$, that NO_2 generation is the result of NO reduction of PdO_2 to PdO [34], and that NO is trapped in the form of $Pd(NO_3)_2$. The scheme considers that NO adsorbed on $Z\text{-}Pd^{2+}Z\text{-}$ is the low temperature bound species and nitrates bound to Pd^{2+} cations are the high temperature species [14,37,38]. The analogous overall reaction is as follows:

$$3\ NO + PdO_2 + 1.5O_2 \leftrightarrow Pd(NO_3)_2 + NO_2 \qquad (R29)$$

(Note that R29 = R20 + R21.) Reactions R16 and R24 are similar to reactions R4 and R9 in Scheme I and represent NO adsorption on Pd^{2+} sites, while reactions R23 to R27 involve the combined uptake of both NO and H_2O on the active sites. A key element in this scheme is the reduction of PdO_2 to give NO_2 which is detected during NO uptake. Further NO uptake occurs on PdO (Reaction 21) leading to the formation of nitrates. Based on modeling to be reported elsewhere [31], Scheme II is also able to predict most of the features of the NO uptake, conversion, and release data.

Schemes I and II are able to predict most of the features of the NOx uptake on Pd/SSZ-13 at different experimental conditions. Each scheme is supported by DRIFTS measurements and DFT calculations. The complicating fact is that Pd may exist in all three oxidation states; Pd^{4+}, Pd^{2+} and Pd^{+}. Definitive discrimination between the schemes is ongoing.

3.6. Effect of reductants

Up to this point the reported NO uptake and release data are for the simple feed devoid of CO and hydrocarbons. Actual diesel exhaust contains a large number of components. In this section we report the effect of individual and mixtures of model diesel exhaust components. We have followed the USDRIVE protocol for clean diesel [29] which specifies that the model feed contain H_2, CO, C_2H_4, C_7H_8, and $C_{12}H_{26}$.

3.6.1. H_2, C_7H_8, and $C_{12}H_{26}$

As shown by Jeftić et al. [41], low temperature combustion has high H_2 content and can have a major impact at higher concentrations. The USDRIVE specified H_2 concentration of 100 is rather low in comparison. To that point, an expanded study on the effect of higher H_2 concentration may be warranted. Our experiments reveal that at 100 ppm H_2 has a negligible effect on both the NO uptake and release, as can be seen in Fig. 6a. The NO uptake is similar during the same two regimes as with the simple feed. The NOx desorption profile essentially overlaps with the profile for the simple feed.

A mixture of C_7H_8, and $C_{12}H_{26}$, referred to as "liquid hydrocarbons" (LHCs) with concentrations of 42 and 58 ppm, respectively, was added to the simple feed. Similar to the experiments with H_2, the LHCs are shown to have a negligible effect on the total NO uptake (Fig. 6b). A minor delay in the NO uptake is noted during the fixed temperature regime and the NO approach to its feed value is slightly below the approach for the NO-only feed. On the other hand, a notable difference is apparent during the temperature ramp; There is a shift to higher temperature NOx desorption, as seen during the ~2400s to 3500 s TPD period. Moreover, a sharper desorption peak with a more distinct maximum at 3046 s (415 °C) is evident. These higher molecular weight reductants may have difficulty in completely penetrating the pores of

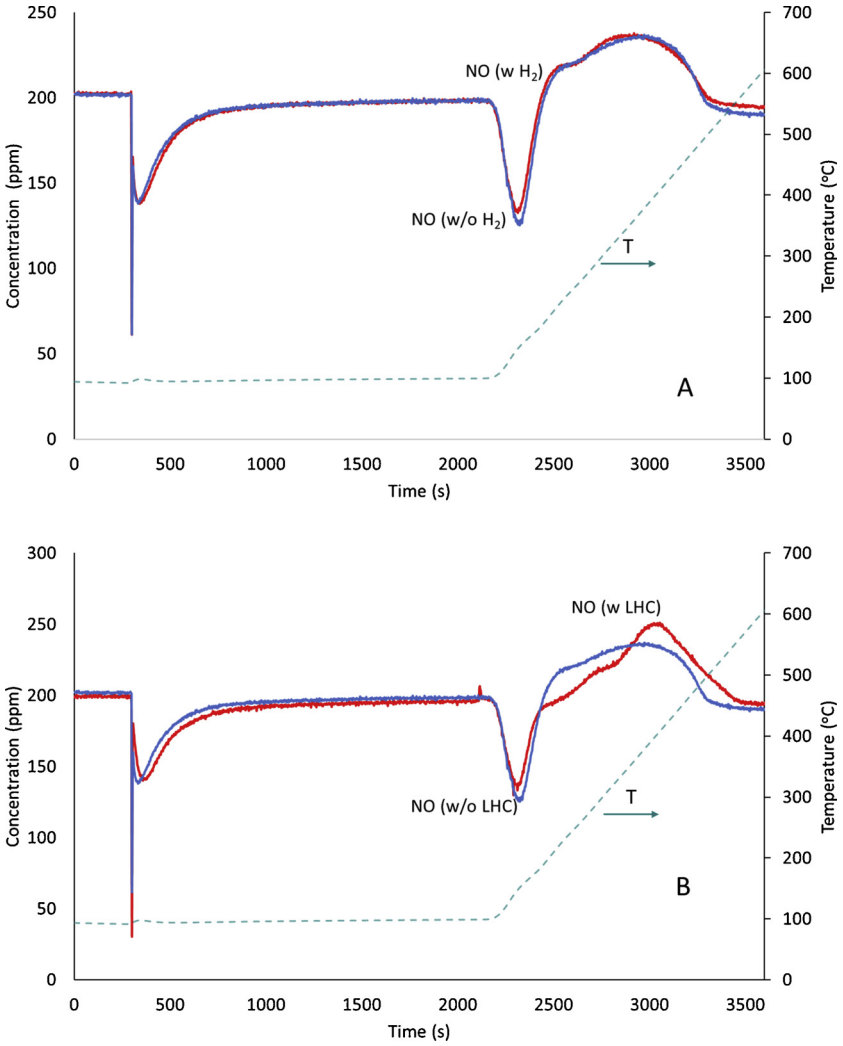

Fig. 6. (a) Hydrogen has no impact on NO adsorption and desorption profile.
Feed: 200 ppm NO, 0 or 100 ppm H_2, 6 % H_2O, 6 % CO_2, 12 % O_2, balance N_2
(b) Delayed adsorption & desorption in presence of Liquid Hydrocarbons (toluene @ 42 ppm + Dodecane @ 58 ppm)
Feed: 200 ppm NO, 0 or 100 ppm LHC, 6 % H_2O, 6 % CO_2, 12 % O_2, balance N_2

the small-pore SSZ-13 zeolite; apparently the small amount that does adsorb serves to inhibit the release of the NO during the TPD. We cannot rule out the possibility that cracked products of dodecane, such as ethylene play a role. A small peak of ethylene was observed at the same temperature range as the high temperature NO peak. Malamis and Harold [42] observed a similar findings in their study of the multi-functional hydrocarbon and NOx trap. A study is currently underway focused on a feed containing dodecane and NO in order to better understand the impact of dodecane on NO desorption behavior.

3.6.2. CO

CO is a known component of diesel engine exhaust and binds to precious metals. We have used a feed concentration of 500 ppm as recommended by the USDRIVE protocol [29]. Like H_2, the CO concentration in advanced low temperature combustion engines may be much higher. The effect of 500 ppm of CO added to the simple feed is shown in Fig. 7. Unlike H_2, CO has a significant impact on the fixed temperature NO uptake at 100 °C. In fact, during the first ~10 s over 98 % of the NO is trapped and over the next ~15 s period about 95 % is trapped. The increase in the low temperature NO uptake is accompanied by a decrease in the higher temperature uptake during the initial part of the temperature ramp. During the remainder of the TPD the NO release generally follows the same trajectory as the simple feed except during a ~600 s period in which the desorbing NO concentration was slightly higher. It is noted that CO_2 rather than NO_2 was observed during NO uptake. We expand on this feature below.

Additional experiments were conducted at several uptake temperatures, with results shown in Fig. 8. A comparison of NO + CO feed (Fig. 8) to the NO-only feed (Fig. 2) indicates similar trends. For both experiments there are four regimes of interest. During the first regime encountered during the initial part of the fixed temperature uptake, an increasing uptake temperature leads increased NO uptake. This is accompanied by a decreased uptake in the second regime during the initial part of the ramp. Fig. 8b shows the NOx trapping efficiency as a function of time during the 300 s fixed temperature uptake period. At the two higher uptake temperatures of 100 and 130 °C, η_T is nearly 100 % for ~10 s and ~50 s, respectively. Further, η_T exhibits a sharp increase at short times between 70 and 100 °C. We return to this point later. In the second regime encountered at ~2300s additional NO uptake occurs, likely a result of H_2O desorption (Fig. S7). The third regime involving NO desorption resembles that with the simple feed over a ~1000s period. The fourth regime is high temperature NO oxidation with features similar to that of the NO-only feed.

The expanded part of Fig. 8a shows NO desorption during the temperature ramp. It is interesting to note that desorption occurs at a somewhat lower temperature for NO that is trapped at 70 °C and 85 °C

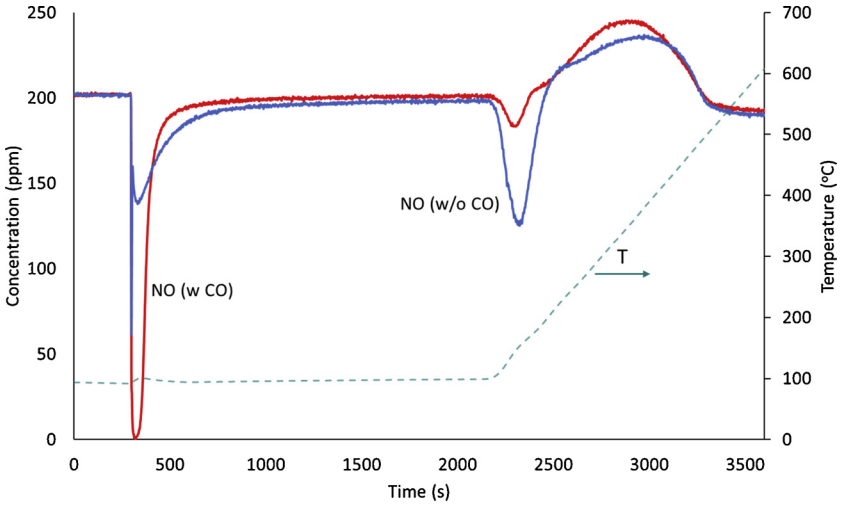

Fig. 7. Impact of CO on NO uptake and release.
Feed: 200 ppm NO, 0 or 500 ppm CO, 6 % H_2O, 6 % CO_2, 12 % O_2, balance N_2

compared to NO that is trapped at the higher temperatures of 100 °C and 130 °C. Comparing these to the NO-only feed it is seen that lower temperature uptake, i.e. 70 °C and 85 °C, in the presence of CO leads to a lower desorption temperature. In contrast, higher temperature NO uptake in the presence of CO leads to desorption curves similar to the NO-only feed. This may suggest a different mechanistic scheme for NO uptake altogether. We return to the mechanism below after considering DRIFTS measurements.

Fig. 9 shows the temporal variation of DRIFTS spectra for CO + NO adsorption on the 1 %Pd/SSZ-13 powder at 100 °C for a dry feed. Shown for comparison is the NO-only spectra (blue). Table 3 lists the IR peaks that have been reported previously for the NO + CO feed on Pd/SSZ-13. During the temporal response following admission of CO a decrease in the 2170 cm^{-1} peak occurs. This is accompanied by an increase in a 2150 cm^{-1} band. This trend suggests the co-adsorption of CO or displacement of NO by CO on the Brønsted acid sites [40]. Khivantsev et al. [43] reported that during vacuum treatment the original bands are restored, which suggests CO binding on the BAS is weaker in comparison to NO. Peaks at 1643 cm^{-1} and 3610 cm^{-1} that are observed for the NO-only feed remain for the NO + CO feed. The strong binding of H_2O serves to eliminate the 2170 $cm^{-1}$to 2150 cm^{-1} peaks during CO addition. Finally, a new feature obtained with the NO + CO feed is the merging of the 1865 cm^{-1} and 1805 cm^{-1} peaks into a single peak at ~1800 cm^{-1}. This feature may suggest a single site for NO binding in the presence of CO, such as Pd^+, although the co-adsorption of CO and NO on $[Pd(II)(OH)]^+$ cannot be ruled out. These points are admittedly speculative particularly because the DRIFTS experiments were done for a dry feed.

The combination of uptake + release data and DRIFTS data provide further support for the two redox schemes described earlier. The incremental increase in NO uptake with the addition of CO is attributed to the lower temperature reduction of Pd^{2+} to Pd^+ by CO (or of Pd^{4+} to Pd^{2+}, as discussed later). CO is a stronger reductant than NO, reducing Pd^{2+} at temperatures below 100 °C; for NO only in the feed, the reduction of Pd^{2+} to Pd^+ occurs at temperatures above 100 °C. For the NO-only feed, NO uptake occurs on $[Pd(OH)]^+$, in competition with H_2O. The addition of CO leads to a reduction in Pd^{2+} to Pd^+ forming CO_2 as the reduction product according to the overall reaction:

$$2\,NO + CO + 2Z^-[Pd(II)OH]^+ \leftrightarrow 2\,Z^-Pd^+\,NO + CO_2H_2O \qquad (R30)$$

Pd^+ has a higher binding energy for NO compared to H_2O according to DFT calculations [30]. This results in an increase in NO uptake. As the

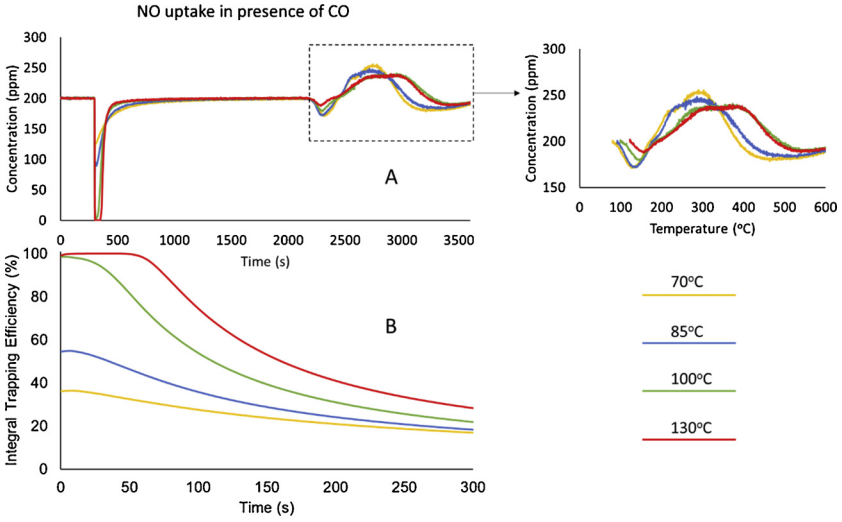

Fig. 8. (a) NO uptake and release for NO + CO feed at several uptake temperatures.
(b) NO trapping efficiency as function of time in presence of CO at several uptake temperatures.
Feed: 200 ppm NO, 0 or 500 ppm CO, 6 % H_2O, 12 % O_2, balance N_2

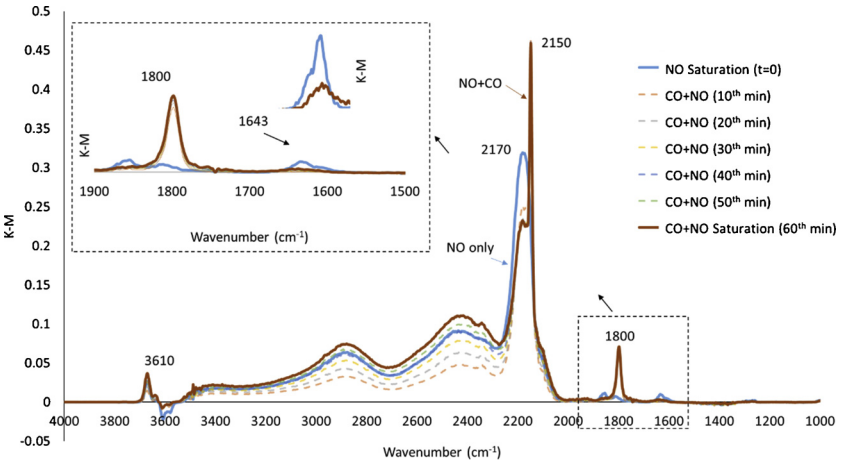

Fig. 9. Evolution of DRIFTS spectra during CO adsorption on NO pre-adsorbed on 1 %Pd/SSZ-13 powder.
Feed: 1400 ppm NO, 3500 ppm CO, 12 % O_2, balance N_2; flow rate = 100 ml/min
Conditions: 100 °C; Duration of 1 h; 50 mg Pd/SSZ-13 powder

uptake temperature is increased from 70 °C to 130 °C, the amount of CO_2 generated increases.

An alternative interpretation for these data is the reduction of Pd^{4+} to Pd^{2+} by the following overall reaction:

$$2\ NO + CO + PdO_2 + 1.5O_2 \leftrightarrow Pd(NO_3)_2 + CO_2 \quad \text{(R31)}$$

Unfortunately, the NO uptake + release date along with the DRIFTS data cannot discriminate between the two proposed reaction schemes.

3.6.3. C_2H_4

C_2H_4 was added at the lower concentration of 200 ppm with NO to assess its impact on NO uptake. The data reveal similar features as for CO (Fig. 10), such as the existence of two uptake periods, one during the fixed temperature and one during the temperature ramp. Further, during the ramp the evolution of water is detected (not shown here). As was done for NO-only and NO + CO feeds, several uptake experiments were conducted for the NO + C_2H_4 at different temperatures (Fig. 11a). NO uptake increases in the lower temperature regime while the uptake decreases in the second regime (Fig. 11). As for the other feeds, four regimes are evident with the similar trends in NO uptake (regimes 1 and 2), release (regime 3), and oxidation (regime 4). Compared with CO at 500 ppm, C_2H_4 at 200 ppm is not as effective in increasing the NO uptake. Fig. 11b shows the dependence of η_T on temperature for the NO + C_2H_4 co-feed. Similar to CO, the addition of C_2H_4 results in a much higher η_T compared to NO alone.

A more detailed examination of the effluent stream composition reveals the formation of acetaldehyde (CH_3CHO) when the NO + C_2H_4 mixture is fed to the Pd(1 %)/SSZ-13 sample. Fig. 12a compares the NO + C_2H_4 co-feed to the C_2H_4-only feed. The evolution of CH_3CHO is noted during the beginning of the NO uptake. A second peak of CH_3CHO along with a second NO uptake is noted during the initial part of the temperature ramp. The evolution of CH_3CHO parallels that of NO_2 evolution for the NO-only feed (Fig. 2) and CO_2 evolution for the NO + CO co-feed (Fig. S9). Adding ethylene to each of the schemes, the following overall reactions are suggested. For Scheme I we have

$$2\ NO + C_2H_4 + 2Z^-[Pd^{2+}(II)OH]^+ \leftrightarrow 2\,Z^-Pd^+\ NO + C_2H_4\ O + H_2O \quad \text{(R32)}$$

while for Scheme II we have

$$2\ NO + C_2H_4 + PdO_2 + 1.5O_2 \leftrightarrow Pd(NO_3)_2 + C_2H_4O \quad \text{(R33)}$$

To examine the role of C_2H_4 and evolution of CH_3CHO in more detail, the same experiment was carried out without NO in the feed. Fig. 12a shows the interesting result that negligible CH_3CHO is formed without NO compared to its immediate generation in the presence of NO. In fact, the CH_3CHO concentration follows the same low level

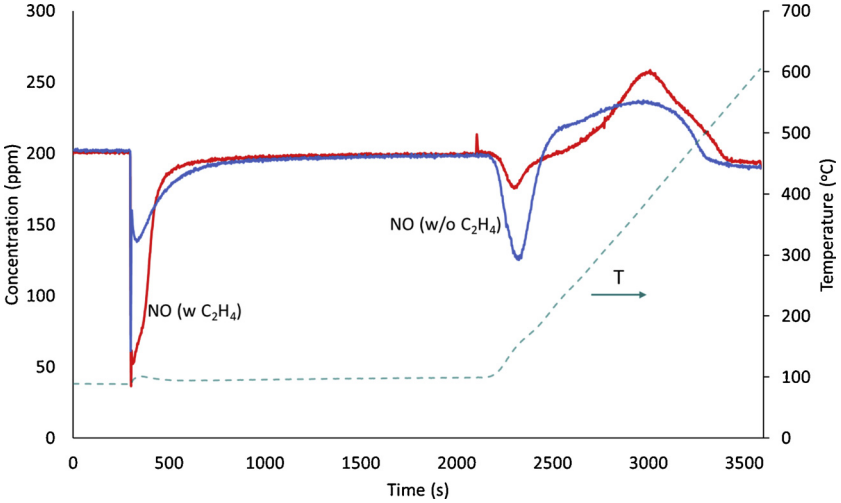

Fig. 10. Impact of C_2H_4 on NO uptake and release.
Feed: 200 ppm NO, 0 or 200 ppm C_2H_4, 6 % H_2O, 6 % CO_2, 12 % O_2, balance N_2

ARTICLE IN PRESS

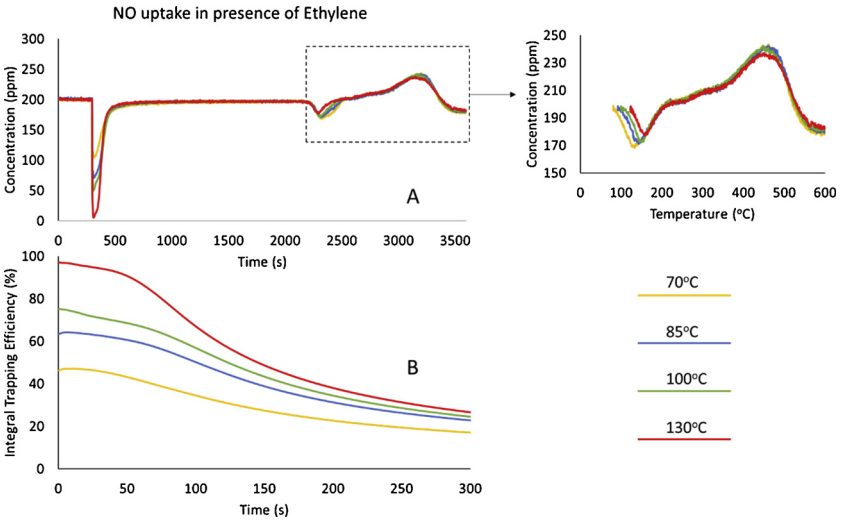

Fig. 11. (a) NO uptake and release for NO + C_2H_4 feed at several uptake temperatures.
(b) NO trapping efficiency as function of time in presence of C_2H_4 at several uptake temperatures.
Feed: 200 ppm NO, 0 or 200 ppm C_2H_4, 6 % H_2O, 12 % O_2, balance N_2

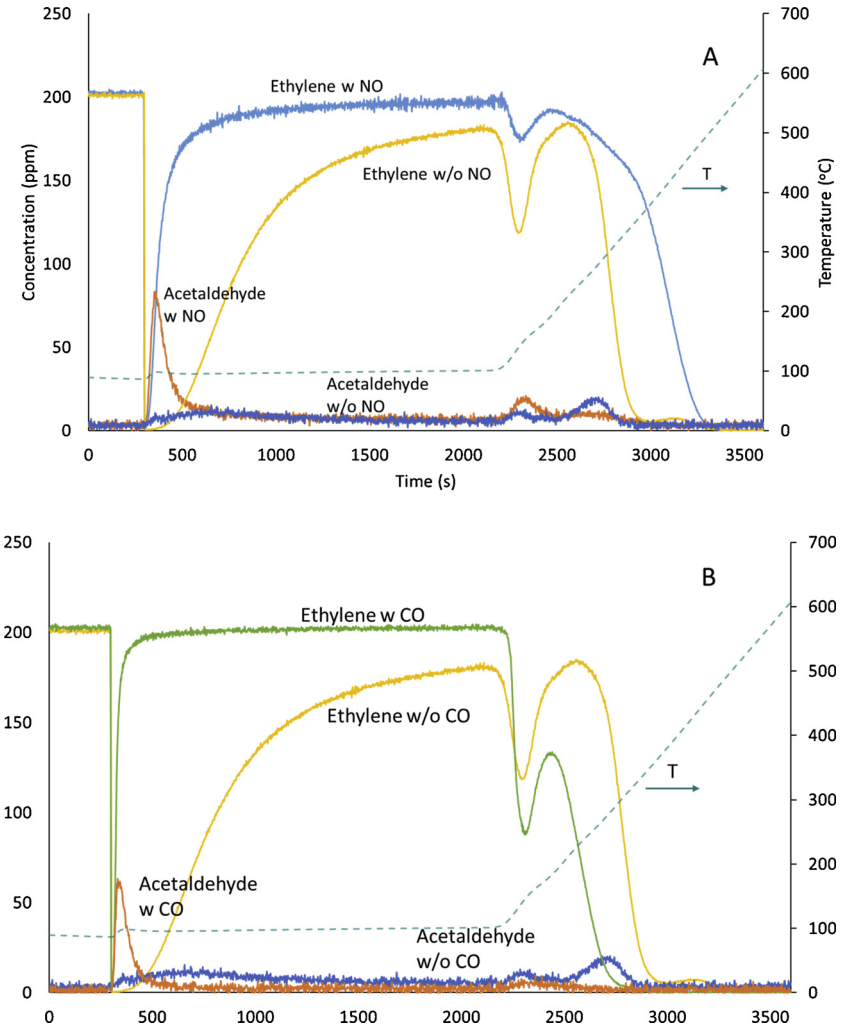

Fig. 12. (a) C_2H_4 uptake and release and CH_3CHO generation with and without NO in feed.(b) C_2H_4 uptake and release and CH_3CHO generation with and without CO in feed. Feed: 0 or 200 ppm NO, 0 or 500 ppm CO, 200 ppm C_2H_4, 6 % H_2O, 12 % O_2, balance N_2.

generation throughout the remainder of the uptake period as for the NO + C_2H_4 feed. These features suggest that NO minimally serves as a promotor for the oxidation of C_2H_4 and formation of CH_3CHO. Concurrent isotopically-labeled TAP experiments to be reported elsewhere suggest that NO is in fact the source of the O [30]. Another experiment was conducted in which C_2H_4 was fed with CO (at 500 ppm) and the result was compared to a feed with C_2H_4 only. The C_2H_4 + CO co-feed data shown in Fig. 12b reveal the formation of an initial evolution of CH_3CHO followed by a decline to a negligible level. It is noted that CO being a stronger reductant forms more CO_2 in comparison to CH_3CHO in case of C_2H_4. Again, this compares to the C_2H_4 – only feed in which there was no burst of CH_3CHO but rather the sustained low level formation of CH_3CHO.

Additional experiments were conducted to elucidate the underlying chemistry of CH_3CHO formation when using C_2H_4 as the reductant. In the first experiment O_2 was removed from the feed containing C_2H_4 + NO. The removal of O_2 had no effect on the formation of CH_3CHO, indicating that the oxidation of C_2H_4 involves a different source of oxygen than O_2. The clear candidate is NO. Several experiments were carried out with and without H_2O for the C_2H_4 + NO co-feed. We found that H_2O is required for CH_3CHO formation.

Collectively, these experiments involving C_2H_4 as a reductant suggest a complex redox mechanism. We speculate that NO uptake in the presence of C_2H_4 parallels that with NO-only and NO + CO. Specifically, NO binds to Z^-Pd^{2+} Z^-, Z^- $[Pd(OH)]^+$, and Z^-Pd^+ sites. The role of C_2H_4 is to effect the $Pd^{2+} \rightarrow Pd^+$ reduction as do reductants NO and CO. The generation of the Pd^+ site leads to strongly-bound NO. Specific to C_2H_4, the generation of CH_3CHO is evidence for this reduction, as NO_2 and CO_2 are for NO and CO. The requirement that NO and H_2O be present for CH_3CHO formation suggests an overall reaction as follows:

$$2\,(Z^-[Pd^{2+}(II)OH]^+ - H_2O) + 2\,NO + C_2H_4 \leftrightarrow 2Z^-Pd^+\,NO + CH_3\,CHO + 3H2O \quad \text{(R34)}$$

Obviously, the reaction is more complex and involves multiple steps. Reaction R34 is proposed based on the underlying reaction schemes discussed above and its existence requires further study.

To provide some mechanistic insight, DRIFTS experiments were conducted with a feed containing C_2H_4 + NO + O_2 feed in the presence of H_2O to the 1 %Pd/SSZ-13 powder. Several IR bands relevant to the surface intermediates formed between NO and C_2H_4 in the reaction were detected. Fig. 13 shows the temporal variation of the spectra during NO + C_2H_4 co-adsorption at 100 °C on a NO-saturated 1 %Pd/SSZ-13. Table 3 lists the key peaks during the interaction of NO and C_2H_4 together with Pd/SSZ-13.

The IR spectra for gas phase ethylene has vibrations in the range 2970–3125 cm^{-1}, 1420–1912 cm^{-1} and 950 cm^{-1}; these are respectively assigned to C–H stretching, H-C–H scissoring, and H-C–H wagging vibrations [44]. Abreu et al. [44] suggested that ethylene adsorption takes place between π-electrons of the double bond with Pd cations, along with weak hydrogen bonding interactions (CH—O interactions) with the oxygen atoms of zeolite framework [44].

Temporal variations of the spectra reveal a decrease in the 2170 cm^{-1} peak similar to what was observed with the CO feed. This trend suggests a displacement of NO by C_2H_4 on the Brønsted Acid sites. The peak at 1865 cm^{-1} disappears and a smaller peak at ~1815 cm^{-1} appears. This peak may be associated with NO adsorbed on Pd^+. Broader peaks at ~1680 cm^{-1} and ~1513 cm^{-1} are observed. These peaks may suggest a NO_y – C_2H_4 complex that is formed and is tentatively assigned to C_2H_4 showing H-C–H vibrations with adsorption on BAS [44]. The NO-C_2H_4 complex maybe the starting point of acetaldehyde formation. The 1482 cm^{-1} peak is assigned to (ν12, δCH_2 in-plane) vibrations based on C_2H_4 interactions with the zeolite [44]. The study done by Olbert-Majkut et al. [45] sheds light on photolysis of C_2H_4—HONO complex and gives insights on possible intermediates being formed. The 1587 cm^{-1} peak is tentatively assigned to N=O stretch of 2-Nitrosoethanol. Similarly, the 1187 cm^{-1} peak is assigned to the rocking and torsion of CH_2 and COH while 1226 cm^{-1} is assigned to the COH bending of 2-nitrosethanol [45]. Finally, the 1513 cm^{-1} peak is tentatively assigned to the C–H stretching of C_2H_4.

At this point it is not known the extent to which a surface complex participates directly in the NO trapping and high temperature NO and NO_2 release. Further study is clearly needed.

3.6.4. Full simulated feed

All five of the reductants (H_2, CO, C_2H_4, C_7H_8, $C_{12}H_{26}$) were combined with NO and H_2O at the concentrations shown in Table 2 and fed to the 1 %Pd/SSZ-13 monolith catalyst. Fig. 14 shows the outcome of this full simulated feed uptake and release experiment. Essentially complete uptake of NO was achieved at 100 °C for about 50 s. Fig. 15 compares the trapping efficiency of the full feed to the simple feed (NO), the feed with NO + CO, the feed with CO + C_2H_4. The comparison shows that the full feed results are comparable to those with CO as the lone reductant. Earlier results showed that the H_2, C_7H_8, and C_{12} do not enhance the low temperature NO uptake. It stands to reason that the enhancement observed with the full feed is the result of CO and C_2H_4, such as an enhanced reduction of Pd^{2+} sites.

A series of experiments were conducted at different uptake temperatures spanning 70 °C–130 °C for the full feed. Fig. 16a shows the dependence of the NO trapping efficiency as a function of time at four

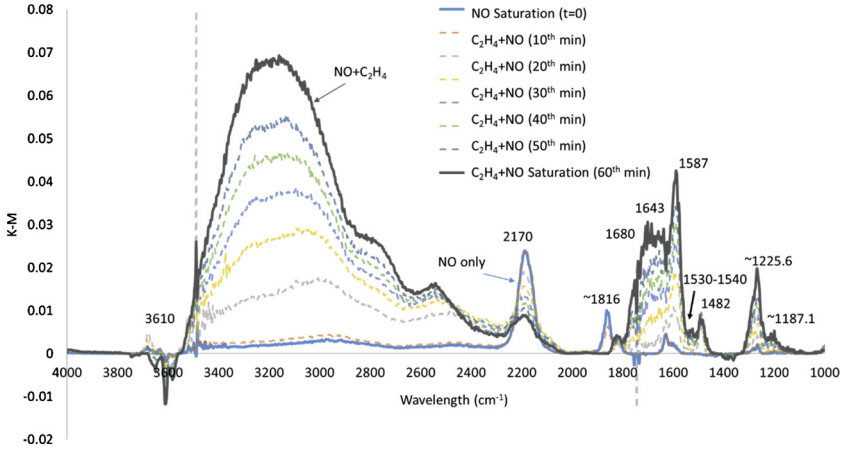

Fig. 13. Evolution of DRIFTS spectra during C_2H_4 adsorption on NO pre-adsorbed on 1 %Pd/SSZ-13 powder at 100 °C.
Feed: 1400 ppm NO, 1400 ppm C_2H_4, 3500 ppm CO, 12 % O_2, balance N_2; flow rate = 100 ml/min
Conditions: 100 °C; Duration of 1 h; 5 mg Pd/SSZ-13 powder

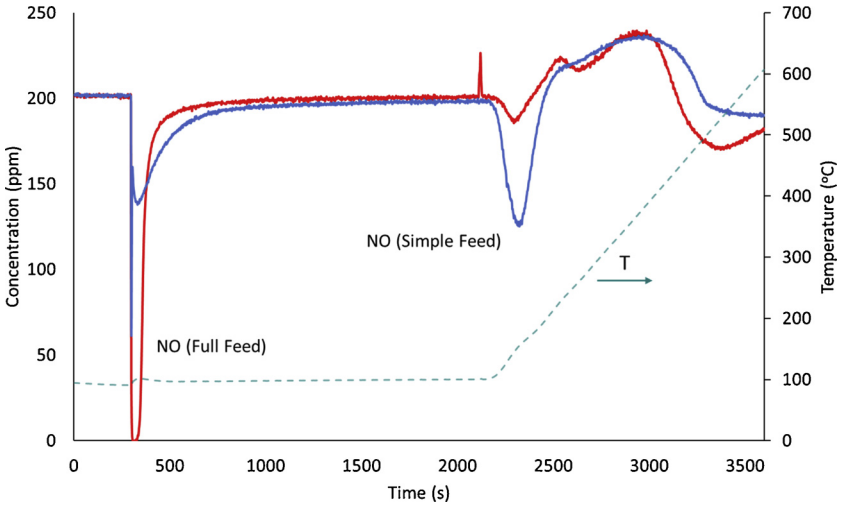

Fig. 14. NO uptake and release for full feed mixture.
Feed: 200 ppm NO, 100 ppm H_2, 100 ppm LHC, 500 ppm CO, 200 ppm C_2H_4, 6 % H_2O, 6 % CO_2, 12 % O_2, balance N_2

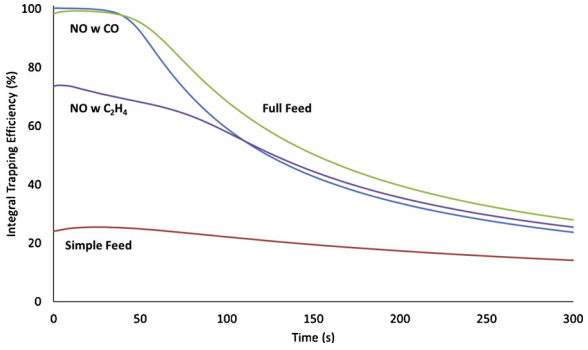

Fig. 15. Comparison of integral trapping efficiency for simple feed (NO only), NO + CO (500 ppm), NO + C_2H_4 (200 ppm) and full feed (see Fig. 14 caption).

uptake temperatures between 70 and 100 °C. The results show that the NO breakthrough time, defined as the time at which η_T decreases below 100 %, is longest (~ 95 s) at the highest temperature of 130 °C. The breakthrough time decreases to ~40 s at an uptake temperature of 100 °C. A further decrease in the temperature results in η_T decreasing below 100 % for all times. An interesting trend is observed for the 100 °C and 85 °C uptake data: The η_{100} intersects the η_{85} curve at ~50 s, implying that more NO is trapped at short times at 100 °C, but more NO is trapped at longer times at 85 °C. This nonlinear trend suggests a complex interplay between the adsorbing species – NO, H_2O, C_2H_4, and CO – and deserves a closer examination.

As shown earlier, only reductants CO and C_2H_4 have a measurable enhancing impact on the NO uptake at 100 °C (Figs. 8 and 11). To this end, a series of uptake experiments were conducted for several combinations of feed components and uptake temperatures, while quantifying the NO trapping efficiency. Specifically compared are the following feeds: NO only, NO + CO, NO + C_2H_4, all in the presence of H_2O at 6 %, and in the 70–100 °C temperature range. Fig. 16b shows the results of these experiments. The data show the general trend that for feeds containing NO + CO (red curves) and NO + C_2H_4 (green curves), the NO trapping efficiency increases monotonically with temperature over the entire 300 s time period. However, it is interesting to note that the increase is nonlinear. For example, for NO + CO there is a large increase in η_T between 85 and 100 °C for short times. Specifically, η_{85} (t → 0) ~ 55 % and η_{100} (t → 0) ~ 100 %. In contrast, for NO + C_2H_4 the increase is more gradual in this temperature range; i.e., η_{85} (t → 0) ~ 63 % and η_{100} (t → 0) ~ 75 %, while a steeper jump occurs at higher

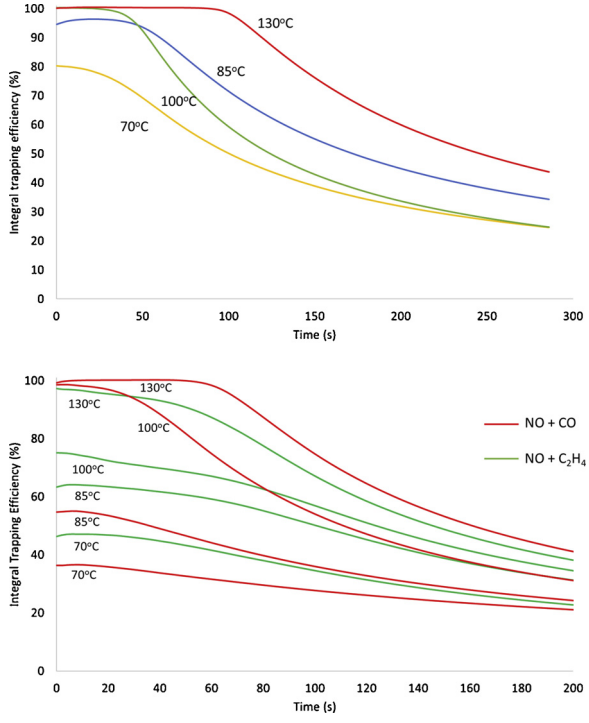

Fig. 16. (a) Effect of uptake temperatures on integral NO trapping efficiency for full feed. Feed: 200 ppm NO, 100 ppm H_2, 100 ppm LHC, 500 ppm CO, 200 ppm C_2H_4, 6 % H_2O, 6 % CO_2, 12 % O_2, balance N_2.
(b) Integral trapping efficiency for different feeds at uptake temperatures.
Feed: 200 ppm NO, 0 or 500 ppm CO, 0 or 200 ppm C_2H_4, 6 % H_2O, 6 % CO_2, 12 % O_2, balance N_2.

temperature; i.e., η_{100} (t → 0) ~ 75 % and η_{130} (t → 0) ~ 95 %. These differences suggest that for the concentrations used CO is more inhibiting than C_2H_4 at 100 °C whereas C_2H_4 is more inhibiting at 85 °C. This leads to the intersection. Further, the drop in η_{100} with time for NO + CO is steeper than for NO + C_2H_4. A steeper decline suggests a stronger coupling between the NO and CO than between NO and C_2H_4. Collectively these differences help to explain the nonlinear behavior observed with the full feed (Fig. 16a).

4. Conclusions

The development of PNA catalysts could significantly reduce automotive exhaust emissions through the reduction of released pollutants during cold-start. This experimental study establishes the potential that Pd/SSZ-13 catalysts has as passive NOx adsorption absorber material.

Bench-scale reactor experiments were carried out to measure the capability of 1 %Pd/SSZ-13 as a PNA material and to provide a deeper understanding of the underpinning mechanism. NOx storage and TPD experiments were run at several uptake temperatures, under dry and wet conditions, and with each individual reductant of a simulated diesel engine exhaust. The experimental findings demonstrate that Pd/SSZ-13 is an effective NO trap in the presence of a non-NO reductant. The presence of H_2O in the feed significantly lowers NOx uptake as a result of competition for sites between H_2O and NOx species and the extent of inhibition is a function of temperature. The data also show clear evidence for the reduction of Pd during the NO uptake. This occurs for the NO-only feed but is enhanced at lower temperature for reductants CO and C_2H_4. The results of temperature ramp experiments that simulate the vehicle warmup reveal NOx desorption at higher temperatures when reductants are present.

The study of Pd/SSZ-13 materials provide insightful data on understanding the mechanisms underlying the NO adsorption. At this point, it is not possible to discriminate between two proposed mechanistic schemes. Suffice it to say, Pd may indeed exist in all three oxidation states – Pd^{4+}, Pd^{2+}, and Pd^{+}. Further research is necessary to flesh out a comprehensive understanding of altering catalyst compositions and the impacts of complicated exhaust emissions.

CRediT authorship contribution statement

Abhay Gupta: Methodology, Investigation, Writing - original draft. **Sung Bong Kang:** Methodology, Investigation, Writing - review & editing. **Michael P. Harold:** Conceptualization, Funding acquisition, Investigation, Methodology, Project administration, Resources, Supervision, Writing - review & editing.

Declaration of Competing Interest

The authors declare that they have no known competing financial interests or personal relationships that could have appeared to influence the work reported in this paper.

Acknowledgements

We acknowledge the financial support of this research by the Department of Energy (DE- EE0008233). We also thank Johnson Matthey, Inc. for supplying the monolith samples for testing. We also acknowledge the helpful discussions with the members of the research groups of Dr. Harold and Dr. Lars Grabow.

Appendix A. Supplementary data

Supplementary material related to this article can be found, in the online version, at doi:https://doi.org/10.1016/j.cattod.2020.01.018.

References

[1] I. Song, S. Youn, D.H. Kim, Characteristics of manganese supported on hydrous titanium oxide catalysts for the selective catalytic reduction of NOx with Ammonia, Top. Catal. 59 (2016) 1008–1012, https://doi.org/10.1007/s11244-016-0582-2.

[2] I. Song, S. Youn, H. Lee, D.H. Kim, CeO_2-TiO_2 catalyst prepared by physical mixing for NH_3 selective catalytic reduction: evidence about the migration of sulfates from TiO_2 to CeO_2 via simple calcination, Korean J. Chem. Eng. 33 (2016) 2547–2554, https://doi.org/10.1007/s11814-016-0112-8.

[3] S.D. Yim, S.J. Kim, J.H. Baik, I.S. Nam, Y.S. Mok, J.H. Lee, B.K. Cho, S.H. Oh, Decomposition of urea into NH_3 for the SCR process, Ind. Eng. Chem. Res. 43 (2004) 4856–4863, https://doi.org/10.1021/ie034052j.

[4] Y. Zheng, D. Luss, M.P. Harold, Optimization of LNT-SCR dual-layer catalysts for diesel NOx emission control, SAE Int. J. Engines. 7 (2014), https://doi.org/10.4271/2014-01-1544.

[5] S.G. Lee, H.J. Lee, I. Song, S. Youn, D.H. Kim, S.J. Cho, Suppressed N_2O formation during NH_3 selective catalytic reduction using vanadium on zeolitic microporous TiO_2, Sci. Rep. 5 (2015) 1–7, https://doi.org/10.1038/srep12702.

[6] L. Ma, Y. Cheng, G. Cavataio, R.W. McCabe, L. Fu, J. Li, In situ DRIFTS and temperature-programmed technology study on NH_3 SCR of NOx over Cu-SSZ-13 and Cu-SAPO-34 catalysts, Appl. Catal. B Environ. 156–157 (2014) 428–437, https://doi.org/10.1016/j.apcatb.2014.03.048.

[7] J.H. Kwak, D. Tran, J. Szanyi, C.H.F. Peden, J.H. Lee, The effect of copper loading on the selective catalytic reduction of nitric oxide by ammonia over Cu-SSZ-13, Catal. Letters 142 (2012) 295–301, https://doi.org/10.1007/s10562-012-0771-y.

[8] S. Saxena, I. Bedoya, Physical phenomena affecting high load operating limits for HCCI engines and strategies for extending these limits, Prog. Energy Combust. Sci. 39 (2012) 457–488, https://doi.org/10.1016/j.pecs.2013.05.002.

[9] https://www.dieselnet.com/standards/us/ld_t3.php (accessed March 20, 2017).

[10] J.R. Theis, C.K. Lambert, Mechanistic assessment of low temperature NOx adsorbers for cold start NOx control on diesel engines, Catal. Today 320 (2019) 181–195, https://doi.org/10.1016/j.cattod.2017.12.014.

[11] F. McKenna, "NOx trap composition". United States Patent US9005560 B2, 14 April 2015. Google Patents. https://patents.google.com/patent/US9005560.

[12] H. Chen and S. Mulla, "Cold start catalyst and its use in exhaust systems". United States Patent US20120308439 A1, 6 December 2012. Patent Scope. https://patentscope.wipo.int/search/en/detail.jsf?docId=WO2015085300.

[13] R.R. Rajaram, F. M. McKenna, H.Y. Chen, D. Liu, "Noble metal-molecular sieve catalysts" U.S. Patent US20150157982 A1, (2014). Google Patents. https://patents.google.com/patent/US20150157982A1/en.

[14] C. Descorme, P. Gélin, M. Primet, C. Lécuyer, Infrared study of nitrogen monoxide adsorption on palladium ion-exchanged ZSM-5 catalysts, Catal. Letters 41 (1996) 133–138, https://doi.org/10.1007/BF00811479.

[15] J. Lee, J.R. Theis, E.A. Kyriakidou, Vehicle emissions trapping materials: successes, challenges, and the path forward, Appl. Catal. B Environ. 243 (2019) 397–414, https://doi.org/10.1016/j.apcatb.2018.10.069.

[16] Y. Gu, W.S. Epling, Passive NOx adsorber: an overview of catalyst performance and reaction chemistry, Appl. Catal. A Gen. 570 (2019) 1–14, https://doi.org/10.1016/j.apcata.2018.10.036.

[17] O. Mihai, L. Trandafilović, T. Wentworth, F.F. Torres, L. Olsson, The effect of Si/Al ratio for Pd/BEA and Pd/SSZ-13 used as passive NOx adsorbers, Top. Catal. 61 (2018) 2007–2020, https://doi.org/10.1007/s11244-018-1017-z.

[18] D. Mei, F. Gao, J. Szanyi, Y. Wang, Mechanistic insight into the passive NO x adsorption in the highly dispersed Pd/HBEA zeolite, Appl. Catal. A Gen. 569 (2019) 181–189, https://doi.org/10.1016/j.apcata.2018.10.037.

[19] K. Khivantsev, N.R. Jaegers, L. Kovarik, J.C. Hanson, F.F. Tao, Y. Tang, I.Z. Koleva, H.A. Aleksandrov, N. Georgi, Y. Wang, F. Gao, J. Szanyi, Achieving atomic dispersion of highly loaded transition metals in small-pore zeolite SSZ-13: a new class of high-capacity and high- efficiency low temperature CO and passive NOx adsorbers, Angew. Chemie (2018), https://doi.org/10.1002/ange.201809343.

[20] Y.S. Ryou, J. Lee, S.J. Cho, H. Lee, C.H. Kim, D.H. Kim, Activation of Pd/SSZ-13 catalyst by hydrothermal aging treatment in passive NO adsorption performance at low temperature for cold start application, Appl. Catal. B Environ. 212 (2017) 140–149, https://doi.org/10.1016/j.apcatb.2017.04.077.

[21] J. Lee, Y. Ryou, S. Hwang, Y. Kim, S.J. Cho, H. Lee, C.H. Kim, D.H. Kim, Comparative study of the mobility of Pd species in SSZ-13 and ZSM-5, and its implication for their activity as passive NOx adsorbers (PNAs) after hydro-thermal aging, Catal. Sci. Technol. 9 (2019) 163–173, https://doi.org/10.1039/c8cy02088d.

[22] Y.S. Ryou, J. Lee, H. Lee, C.H. Kim, D.H. Kim, Effect of various activation conditions on the low temperature NO adsorption performance of Pd/SSZ-13 passive NOx adsorber, Catal. Today 320 (2019) 175–180, https://doi.org/10.1016/j.cattod.2017.11.030.

[23] Y. Murata, T. Morita, K. Wada, H. Ohno, NOx trap three-way catalyst (N-TWC) concept: TWC with NOx adsorption properties at low temperatures for cold-start emission control, SAE int, J. Fuels Lubr. 8 (2015) 454–459, https://doi.org/10.4271/2015-01-1002.

[24] Y. Zheng, L. Kovarik, M.H. Engelhard, Y. Wang, Y. Wang, F. Gao, J. Szanyi, Low-temperature Pd/Zeolite passive NOx adsorbers: structure, performance, and adsorption chemistry, J. Phys. Chem. C. 121 (2017) 15793–15803, https://doi.org/10.1021/acs.jpcc.7b04312.

[25] A. Vu, J. Luo, J. Li, W.S. Epling, Effects of CO on Pd/BEA passive NOx adsorbers, Catal. Letters 147 (2017) 745–750, https://doi.org/10.1007/s10562-017-1976-x.

[26] Chakarova, Kristina, Ivanova, Elena, Hadjiivanov, Konstantin, D. Klissurski, H. Knözinger, Co-ordination chemistry of palladium cations in Pd-H-ZSM-5 as revealed by FTIR spectra of adsorbed and co-adsorbed probe molecules (CO and NO), J. Chem. Soc. Faraday Trans. 6 (2004) 3702–3709, https://doi.org/10.1039/B401934B.

[27] K. Khivantsev, F. Gao, L. Kovarik, Y. Wang, J. Szanyi, Molecular level understanding of how oxygen and carbon monoxide improve NO x storage in Palladium/SSZ-13 passive NOx adsorbers: the role of NO + and Pd(II)(CO)(NO) species, J. Phys. Chem. C. 122 (2018) 10820–10827, https://doi.org/10.1021/acs.jpcc.8b01007.

[28] B.J. Adelman, W.M.H. Sachtler, The effect of zeolitic protons on NO, reduction over Pd / ZSM-5 catalysts 14 (1997), https://doi.org/10.1016/S0926-3373(97)00007-6.

[29] USDRIVE protocol: 2018_LTAT_Low-Temperature-Storage-Protocol https://cleers.org/low-temperature-protocols/ (accessed Dec. 5, 2019).

[30] U. Menon, B.M.M. Rahman, A. Gupta, L.C. Grabow, M.P. Harold, ACS Catal. (2020)

ARTICLE IN PRESS

to be submitted.
[31] M. Ambast, K. Karinshak, B.M.M. Rahman, L.C. Grabow, M.P. Harold, Passive NOx adsorption on Pd/H-ZSM-5: experiments and modeling, Appl. Catal. B Environ. (2020) in review.
[32] K.S. Kabin, R.L. Muncrief, M.P. Harold, Y. Li, Dynamics of storage and reaction in a monolith reactor: lean NOx reduction, Chem. Eng. Sci. 59 (2004) 5319–5327, https://doi.org/10.1016/j.ces.2004.07.114.
[33] K. Hadjiivanov, J. Saussey, J.L. Freysz, J.C. Lavalley, FT-IR study of NO + O2 co-adsorption on H-ZSM-5: Re-assignment of the 2133 cm-1 band to NO+ species, Catal. Letters 52 (1998) 103–108.
[34] N. Artioli, R.F. Lobo, E. Iglesia, Catalysis by confinement: Enthalpic stabilization of NO oxidation transition states by microporous and mesoporous siliceous materials, J. Phys. Chem. C. 117 (2013) 20666–20674, https://doi.org/10.1021/jp406333d.
[35] J.A. Loiland, R.F. Lobo, Oxidation of zeolite acid sites in NO/O_2 mixtures and the catalytic properties of the new site in NO oxidation, J. Catal. 325 (2015) 68–78, https://doi.org/10.1016/j.jcat.2015.02.009.
[36] H.Y. Chen, J.E. Collier, D. Liu, L. Mantarosie, D. Durán-Martín, V. Novák, R.R. Rajaram, D. Thompsett, Low temperature NO storage of zeolite supported Pd for low temperature diesel engine emission control, Catal. Letters 146 (2016) 1706–1711, https://doi.org/10.1007/s10562-016-1794-6.
[37] I. Perdana, D. Creaser, I. Made Bendiyasa, B. Rochmadi, Wikan Tyoso, Modelling NOx adsorption in a thin NaZSM-5 film supported on a cordierite monolith, Chem. Eng. Sci. 62 (2007) 3882–3893, https://doi.org/10.1016/j.ces.2007.04.012.
[38] T.E. Hoost, K.A. Laframboise, K. Otto, NO adsorption on Cu-ZSM-5: assignment of IR band at 2133 cm^{-1}, Catal. Letters 33 (1995) 105–116, https://doi.org/10.1007/BF00817050.
[39] S. Dzwigaj, L. Lietti, S. Morandi, L. Castoldi, A. Porta, R. Matarrese, T. Pellegrinelli, Low temperature NOx adsorption study on Pd-Promoted zeolites, Top. Catal. 61 (2018) 2021–2034, https://doi.org/10.1007/s11244-018-1045-8.
[40] X. Wang, H. Chen, W.M.H. Sachtler, Selective reduction of NOx with hydrocarbons over Co/MFI prepared by sublimation of $CoBr_2$ and other methods, Appl. Catal. B Environ. 29 (2001) 47–60, https://doi.org/10.1016/S0926-3373(00)00186-7.
[41] M. Jeftić, G.T. Reader, M. Zheng, Impacts of low temperature combustion and diesel post injection on the in-cylinder production of hydrogen in a lean-burn compression ignition engine, Int. J. Hydrogen Energy 42 (2017) 1276–1286, https://doi.org/10.1016/j.ijhydene.2016.11.008.
[42] S. Malamis, M.P. Harold, Optimizing the Lean Hydrocarbon NOx Trap: Sequential and Dual-Layer Configurations, Catal. Today (2020) in press.
[43] K. Khivantsev, N.R. Jaegers, L. Kovarik, S. Prodinger, M.A. Derewinski, Y. Wang, F. Gao, J. Szanyi, Palladium/Beta zeolite passive NOx Adsorbers (PNA): clarification of PNA chemistry and the effects of CO and zeolite crystallite size on PNA performance, Appl. Catal. A Gen. 569 (2019) 141–148, https://doi.org/10.1016/j.apcata.2018.10.021.
[44] N.J. Abreu, H. Valdés, C.A. Zaror, F. Azzolina-Jury, M.F. Meléndrez, Ethylene adsorption onto natural and transition metal modified Chilean zeolite: an operando DRIFTS approach, Microporous Mesoporous Mater. 274 (2019) 138–148, https://doi.org/10.1016/j.micromeso.2018.07.043.
[45] A. Olbert-Majkuta, Z. Mielke, K.G. Tokhadze, Photolysis of the C2H4-HONO complex in low temperature matrices: formation of 2-nitrosoethanol, J. Mol. Struct. 656 (2003) 321–332, https://doi.org/10.1016/S0022-2860(03)00329-6.